

Emission Characteristics and Flame Stability in HEFA Fueled Gas Turbine Combustors



H. Fujiwara, P. Salman, S. Ando, H. Ishikawa, S. Nakaya, M. Tsue, and K. Okai

Nomenclature

ASTM	American Society for Testing and Materials
CO	Carbon monoxide
CO ₂	Carbon dioxide
EI	Emission Index
FAME	Fatty and methyl-ester fuel
FT-SPK	Fischer-Tropsch Synthetic Paraffin Kerosene
HEFA	Hydro-treated Ester and Fatty Acid
ILIDS	Interferometric Laser Imaging Droplet Sizing
JAXA	Japan Aerospace Exploration Agency
KAKENHI	Grants-in-Aid for Scientific Research
LBO	Lean Blow Out
MHPS	Mitsubishi-Hitachi Power Systems
NEDO	New Energy Industrial Technology Development Organization
NO _x	Nitrogen oxides
nvPM	Non-volatile particulate matter
PASS	Photo acoustic soot sensor
Re	Reynolds number
RQL	Rich burn Quick quench and Lean burn
SPK	Synthetic Paraffin Kerosene

H. Fujiwara (✉) · K. Okai

Propulsion Research Unit, Aeronautical Research Directorate, Japan Aerospace Exploration Agency, 7-44-1 Jindaiji-Higashi, Chofu, Tokyo 182-8522, Japan
e-mail: fujiwara.hitoshi@jaxa.jp

P. Salman · S. Ando · H. Ishikawa · S. Nakaya · M. Tsue
Department of Aeronautics and Astronautics, Graduate School of Engineering, The University of Tokyo, 7-3-1 Hongo, Bunkyo, Tokyo 113-8656, Japan

TEC	Toyo Engineering Cooperation
THC	Total hydrocarbons
UOP	Universal Oil Products

1 Introduction

Global climate change due to the rapid increase in CO₂ emissions especially caused by aviation is one of the critical issues that can be solved through international collaborations. Although the amount of CO₂ emissions from aviation consists of only around 2% of the total CO₂ emissions, it is of crucial importance to start suppressing emissions caused by air traffic as early as possible. Recent rapid growth of aviation transportation has caused many activities that could curtail CO₂ reduction from aviation. Much efforts are in progress in other fields, such as electric and hybrid vehicles in the automotive sector and carbon dioxide capture and storage (CCS) installations in power generation plants. It should be noted that more than 90% of CO₂ emissions from commercial aircraft operations are generated by large aircraft, indicating of pursuing research to reduce commercial aircraft emissions with a focus on technology applicable to large commercial aircraft [1].

In aviation, alternative fuels are considered one of the important options to suppress CO₂ emission, while their specifications are strictly defined in ASTM D7566 “Standard Specification for Aviation Turbine Fuel Containing Synthesized Hydrocarbons” [2]. Its Annexes define not only the chemical and physical properties but also the manufacturing process of those fuels, which is of prime importance from the aviation safety point of view.

In our joint research group between JAXA and the University of Tokyo, discussions and investigations of bio-derived aviation alternative fuels started in 2010. At JAXA, the impact of introducing biofuels in turbofan jet engines has been investigated [3] and combustion testing begun with available (not-certified and general) bio-fuel (Fatty acid methyl-ester, FAME fuel) in 2011 [4]. As expected, the fuel had higher CO emissions at low load conditions due to low flame temperature [5].

In 2017, Mitsubishi-Hitachi Power System (MHPS) with partners (Toyo Engineering Cooperation (TEC), Chubu Electric Power and JAXA) started a project to conduct a pilot-scale plant testing on a Fischer-Tropsch Synthetic Paraffin Kerosene (FT-SPK) fuel production derived from lignocellulosic biomass supported by NEDO [6]. For this project, JAXA participated to conduct the final combustion tests of the product. In addition, the University of Tokyo and JAXA conducted fundamental research on biofuels combustion supported by KAKENHI.

This article presents the results of investigations on aviation certified biofuels to understand the limitations and potentials of bio-derived aviation fuels as a contribution towards more environmentally friendly aviation. It further focuses on emission characteristics and flame stability with Jet A1 and HEFA fuels using the same configurations.

The alternative turbine fuel used in this study was hydro-treated ester and fatty acid (HEFA) made from tallow fat, provided by Honeywell UOP/Nikki Universal. The manufacturing process is specified in Annex 2 of ASTM D7566. The HEFA fuel was available for commercial flights if the blending ratio did not exceed 50 vol.% as specified in Annex 2.

Specifications for HEFA are provided in ASTM D7566 Annex 2 [7]. To understand the similarities and differences of HEFA fuel compared to the baseline Jet A1 fuel, the properties of HEFA fuel were analyzed. Table 1 summarizes the result.

2 Combustor Tests and Conditions

2.1 Basic Combustion Tests

Several basic tests were conducted to understand the overall combustion characteristics of the mentioned fuels, including instabilities. Obtained data were analyzed to evaluate important structures of combustion, as well as air and fuel conditions.

Figure 1 shows a schematic and a photograph of one of the tested injectors. Figure 2 shows the experimental apparatus for the measurement of spray droplet diameter distribution, in which spray testing with swirled flow was realized. For the droplet measurement, Interferometric Laser Imaging for Droplet Sizing (ILIDS) was used [8–10].

Test conditions are shown in Table 2.

Single droplet evaporation tests were conducted using an apparatus shown in Fig. 3. The droplet diameter measurement was conducted with the method introduced by Nakaya and co-workers [11] both in normal and microgravity conditions.

Test conditions are shown in Table 3.

Combustion instability experiments with a fuel nozzle configuration such as for droplet diameter measurement were investigated at the University of Tokyo hypersonic and high-temperature wind tunnel. Figure 4 shows a schematic of the test apparatus. High-temperature air from the heater was injected into the experimental apparatus and high pressure was reached due to the choked nozzle further downstream. The flow was exhausted to the building's environment through the silencer tower (not shown in the schematics). CH* Chemiluminescence of the flame and Mie scattering of the spray were taken using high-speed cameras (Vision Research Inc., Micro LC 310, and MiroEx2) at 2000 and 1000 fps, respectively.

Test conditions are shown in Table 4.

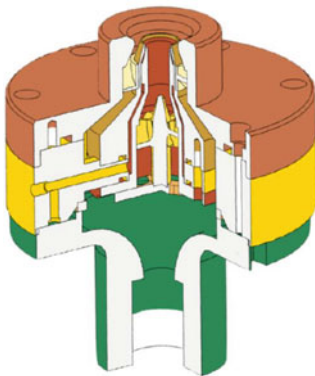
Table 1 Chemical and physical analysis of the fuels

Properties	HEFA	D7566 Table A2.1-2	Jet A1	Jet A1: HEFA = 50:50	D7566 Table 1	Test method
Freezing point (°C)	-58.5	<-40	-48.0	-51.5	<-47	JIS K 2276
Dynamic viscosity (mm ² /s) @ 15 °C	1.963	N/A	1.655	1.786	<8 (-20 °C)	JIS K2283
Surface tension (mN/m)	22.5	N/A	23.6	23.1	N/A	JIS K 2241
Density (g/cm ³) @ 15 °C	0.7554	0.73-0.77	0.7886	0.7732	0.775-0.840	JIS K 2249-1
Net heat of combustion (MJ/kg)	44.14	N/A	43.38	43.73	>42.8	JIS K 2279
<i>Physical distillation</i>						JIS K 2254
Initial boiling point (°C)	146.5	N/A	148.5	148.5	N/A	
10% recovered temp. (°C)	165.0	<205	164.5	165.0	<205	
50% recovered temp. (°C)	208.0	Report	193.5	198.5	Report	
90% recovered temp. (°C)	253.5	Report	237.5	247.0	Report	
Final boiling point (°C)	269.0	<300	259.0	262.0	<300	
Lubricity (mm)	1.04	N/A	0.83	0.87	<0.85	ASTM D5001
Carbon (mass%)	84.7	N/A	86.1	85.4	N/A	JPI-5S-65
Hydrogen (mass%)	15.2	N/A	13.8	14.5	N/A	
Sulfur (mass%)	<0.0001	<0.0015	0.0006	0.0003	<0.3	JIS K 2541-6
<i>Composition</i>						ASTM D1319
Paraffin (vol.%)	98.4	Report	79.1	89.1	N/A	

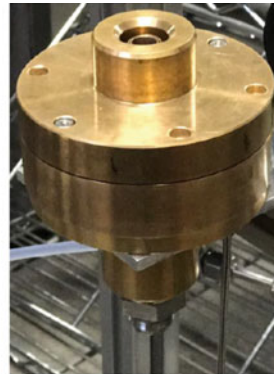
(continued)

Table 1 (continued)

Properties	HEFA	D7566 Table A2.1-2	Jet A1	Jet A1: HEFA = 50:50	D7566 Table 1	Test method
Olefin (vol. %)	0.9	N/A	3.0	1.6	N/A	
Total aromatics (vol.%)	0.7	N/A	17.9	9.3	8-25	
<i>Aromatics</i>						ASTM D6379
Benzenes (vol.%)	<0.1	N/A	19.1	10.2	N/A	
(mass%)	<0.1	N/A	21.3	11.6	N/A	
Naphthalene (vol.%)	<0.1	N/A	0.1	0.1	N/A	
(mass%)	<0.1	N/A	0.2	0.1	N/A	
Total aromatics (vol.%)	<0.1	N/A	19.2	10.3	8.4–26.5	
(mass%)	0.1	N/A	21.5	11.8	N/A	



(a) Schematic view



(b) Photograph

Fig. 1 Double-swirl air-blast fuel nozzle

2.2 Single Sector Combustor Testing at JAXA Combustion Test Rig

Two types of single-injector combustors were used for testing at JAXA AP7 medium-pressure test rig, with the maximum inlet temperature, pressure, and air-mass flow of 1000 K, 10 bar and 2 kg/s, respectively. Figure 5 shows the schematic of the test facility showing especially the air supply system.

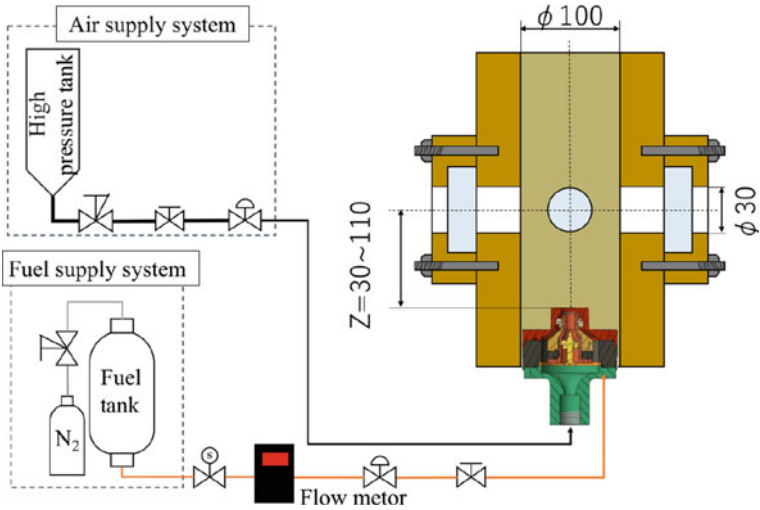
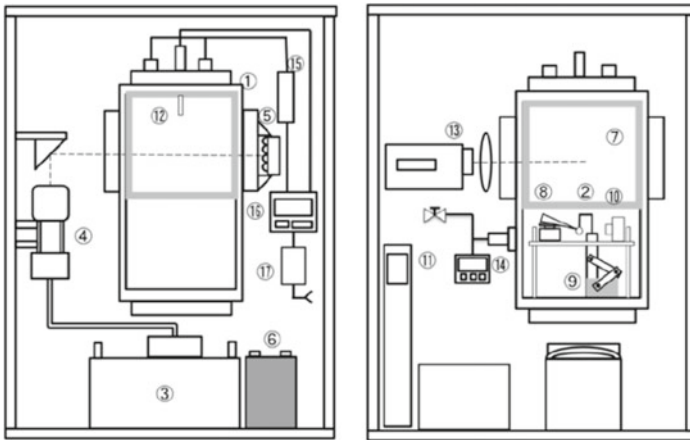


Fig. 2 Schematic of the experimental apparatus for droplet size measurement of a double-swirl injector at atmospheric condition

Table 2 Droplet diameter measurement test condition

Case	Air flow rate	Swirl number	Equivalence ratio	Fuel
B1	15 (g/s)	0.13	0.71	Jet A1, HEFA



- ① Combustion chamber, ② Silica fiber, ③ High-speed camera, ④ Camera head, ⑤ LED back light, ⑥ 12V battery, ⑦ Electric furnace, ⑧ Glass tube, ⑨ Servomotor, ⑩ Camera, ⑪ UPS, ⑫ Thermocouple, ⑬ Video camera, ⑭ Pressure measurement, ⑮ Solid state relay, ⑯ Temperature controller, ⑰ Circuit breaker

Fig. 3 Droplet evaporation test apparatus

Table 3 Single droplet evaporation test condition

Case	Temperature	Pressure	Gas composition	Fuel
B2	750 °C	Ambient pressure	Nitrogen 100%	Jet A1, HEFA

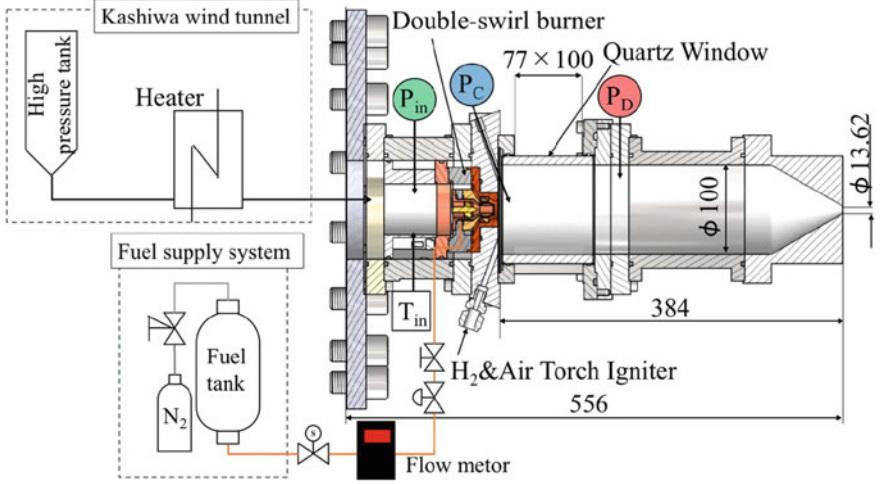


Fig. 4 Schematic of the experimental apparatus for double-swirl injector combustion testing at high pressure and temperature condition

Table 4 Test condition for high-temperature and pressure combustion at University of Tokyo combustion wind tunnel

Case	Air temperature	Air pressure	Equivalence ratio	Fuel
B3	600 K	500 kPa	0.71	Jet A1, HEFA

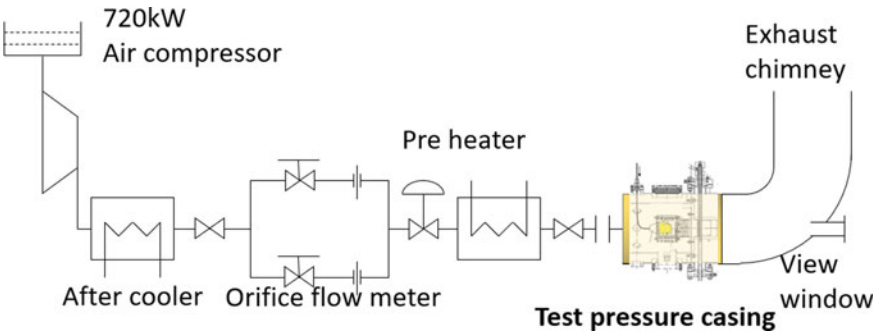


Fig. 5 Schematic of JAXA AP7 medium-pressure test rig (air supply system)

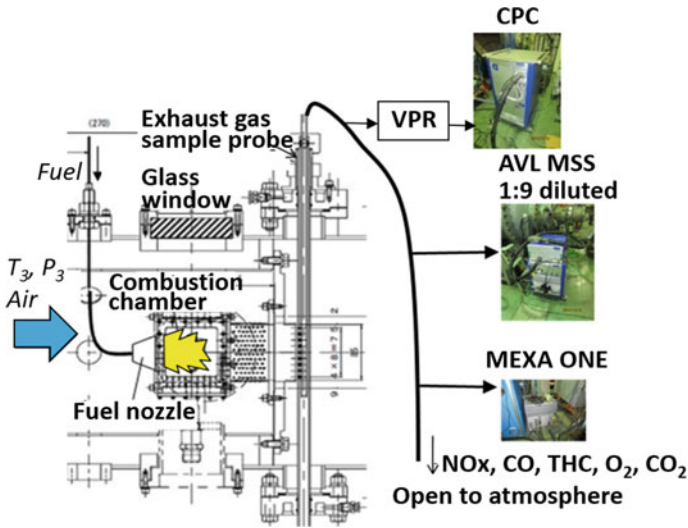


Fig. 6 Combustion test pressure casing overview

Whole test chambers are installed in a test pressure casing retractable from the facility to hold several different types of combustion chambers. Figure 6 shows an enlarged image of the pressure casing portion. The tested combustion chamber is installed in a pressure casing and connected to the fuel supply system. Cables from the measurement equipment are connected via the pressure casing.

This test rig is usually used for the demonstration of new combustor concepts and for the development of innovative measurement technologies. Crystal glass windows were installed in both the facility pressure casing and the combustor liner so that the high-pressure combustion phenomena can directly be observed from outside of the casing (see Fig. 7). An exhaust gas sample probe with eight $\psi 0.8$ mm sampling holes was located at the exit of the combustor liner (Fig. 7).

The samples from the exhaust gas were led to the measurement instruments through a stainless-steel tube connected to a valve to control the mass flow and temperature of the sample gas. NO_x concentration was measured using a chemiluminescence detector (CLD), CO, and CO_2 concentrations were measured through nondispersive infrared detectors (NDIR), and total hydrocarbon (THC) concentration was measured using a flame ionization detector (FID), Horiba MEXA ONE. Non-volatile particle matter (nvPM) mass concentration was measured using a photoacoustic soot sensor (PASS), AVL MSS 483. The number of nvPM was also measured through a condensation particle counter (CPC) with a particle remover (VPR). A condensation particle counter (CPC) is a particle counter that detects and counts aerosol particles by first enlarging them and using the particles as nucleation centers to create droplets in a supersaturated gas (see Fig. 8). In this study, nucleation is accomplished through thermal diffusion (working gas is n-butanol).

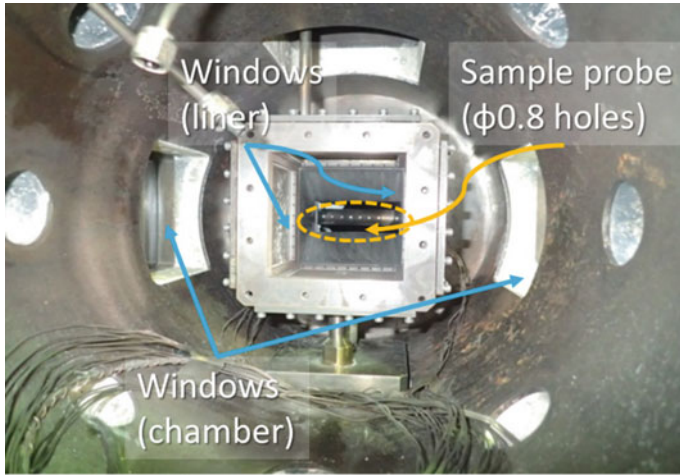


Fig. 7 View inside the pressure casing (viewed from upstream)

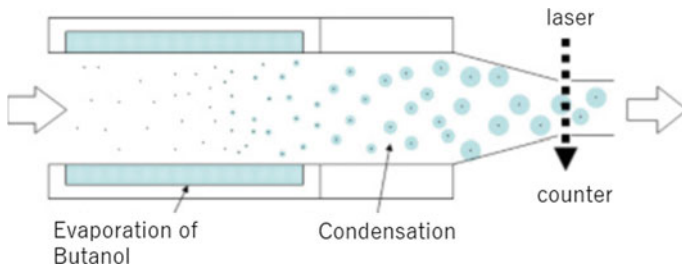


Fig. 8 Schematic of a condensation particle counter (CPC)

Spatial distribution of soot concentration was estimated using Hottel and Broughton two-color radiometry [12].

One of the tested combustors (case 1) was a RQL combustor [13] as shown in Fig. 9, wherein 10% of total air flow entered through the upstream Parker-Hannifin type air-blast fuel nozzle [5] (Fig. 10), while the remaining 90% of total air entered through the air holes located on the combustor liner (seen in Fig. 9 as combustion/dilution air holes). The other combustor (case 2) was a concentric lean-burn burner [14] as seen in Fig. 11, which consisted of a pilot diffusion burner located at the center and a lean premix main burner surrounding it. Only the pilot burner was fueled at low load inlet air condition, while at high load conditions both pilot and main burner were fueled.

Combustion tests were performed for the conditions shown in Table 5.

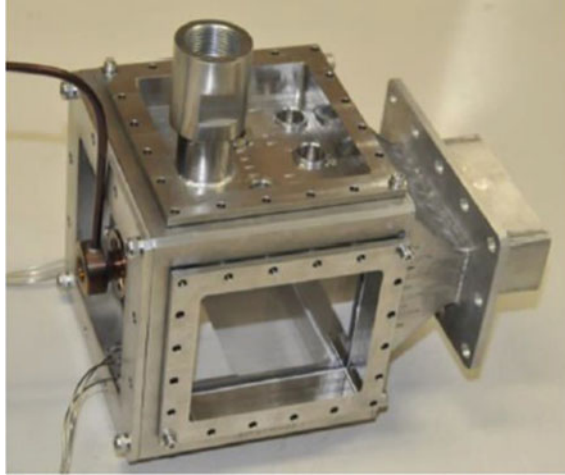


Fig. 9 Test chamber for RQL combustor

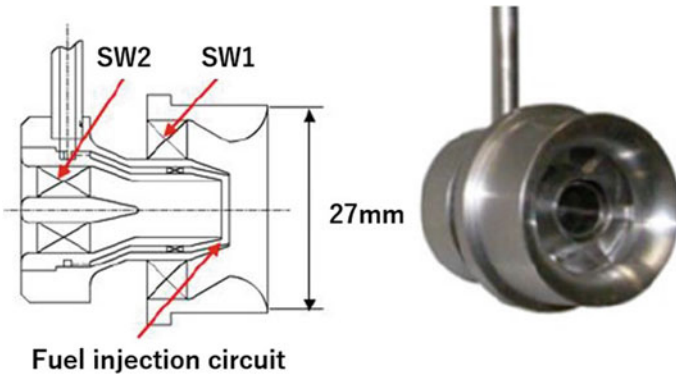


Fig. 10 Parker-Hannifin type air-blast fuel nozzle [13]

3 Results

3.1 Results of Basic Combustion Testing

To investigate the spray shape and structure in measurement locations, Mie scattering image was taken in the atmospheric pressure combustion test apparatus. Figure 12 shows the Mie scattering image for the same condition as droplet diameter distribution measurement shown in Table 2 (fuel was Jet A1). Time-averaged CH* chemiluminescence images for the two fuel were shown in Fig. 13. Squares in Figs. 12 and 13 indicate the locations of the ILIDS measurements.

Fig. 11 Concentric lean burn burner

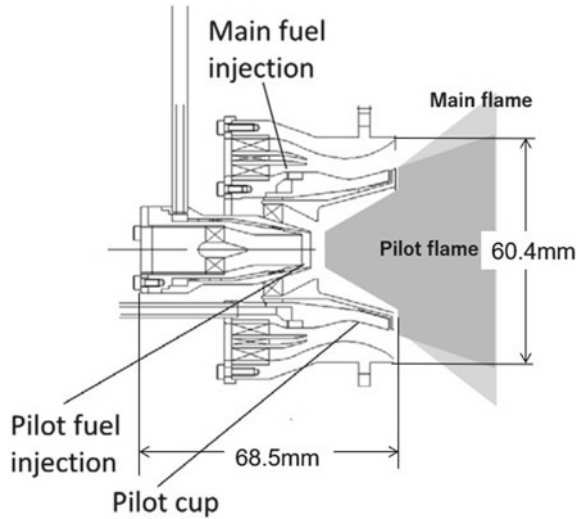


Table 5 JAXA combustion rig test conditions

Case	Combustor	Inlet temperature (K)	Inlet pressure (kPa)	Pressure loss ratio (%)	Fuel injection type
1-1	RQL	450	350	4.0	N/A
1-2		500	500	4.0	N/A
1-3		550	800	4.0	N/A
2-1	Lean burn	450	360	4.0	Pilot only
2-2		760	700	4.0	Pilot + main (pilot = 20%)
2-3		760	700	4.0	Pilot + main (pilot = 15%)

Mie scattering image shown in Fig. 12 suggests that spray flame relatively distributes near the center line from the injector exit. The density of the spray decreases with the distance downstream from the injector exit, and most of the spray droplets evaporate around $Z = 50\text{--}70$ mm. The location is close to the lifted flame position as seen in Fig. 13. These observations suggest that the spray distribution in the test configuration and condition is nearly 1-dimensional along the center line. In this sense, the selected ILIDS measurement points cover unburned, flame, and burned regions, and the selected measurement positions are adequate to investigate the atomization, evaporation, and combustion processes.

Figure 14 shows an example of droplet diameter distribution measurement using ILIDS. Each droplet is represented by an interference fringe and the fringe number accounts for the droplet diameter scaling.

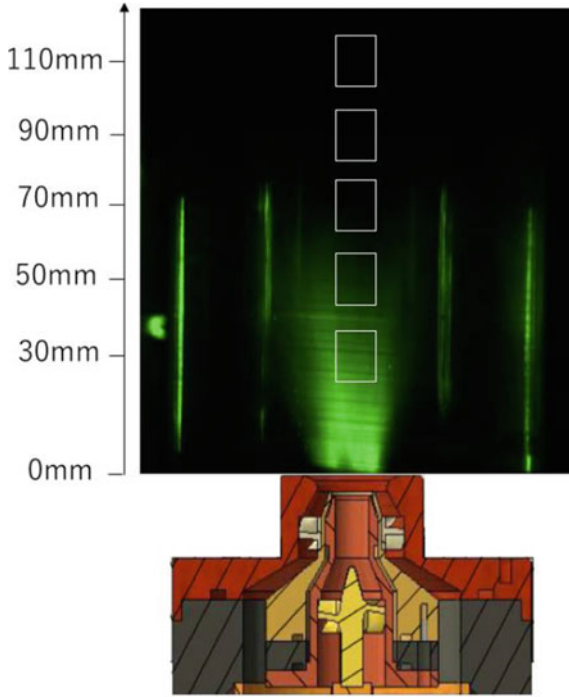


Fig. 12 Spray scattered image (fuel: Jet A1)

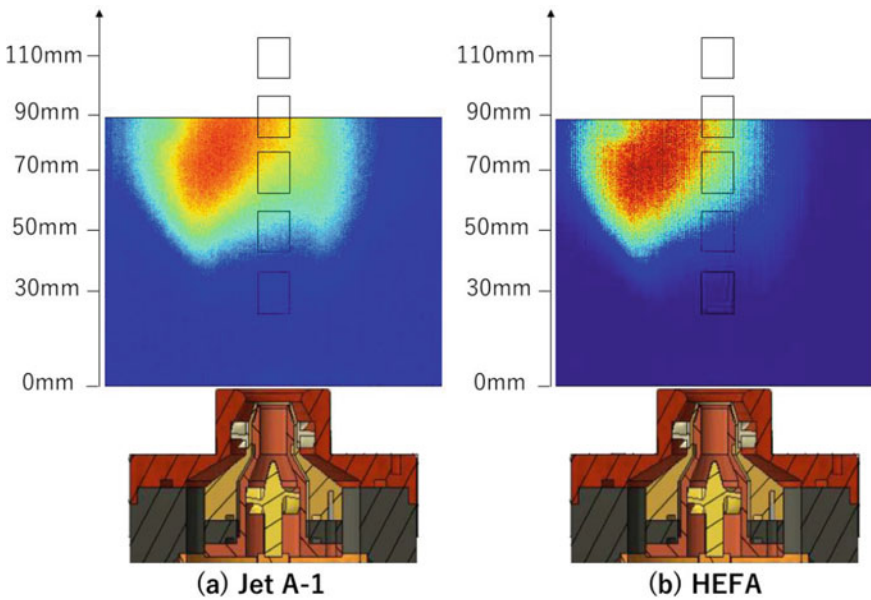


Fig. 13 Time-averaged image of CH* chemiluminescence

Fig. 14 Example of ILIDS measurement



Figure 15 shows droplet diameter distribution at 30 mm downstream from injector exit both for Jet A1 (a) and HEFA (b) fuels. The location is well upstream from a flame location indicated in Fig. 13 and atomization characteristics can be compared between the two fuels. Measured Sauter Mean Diameter indicated in Fig. 15 was slightly larger for cases using HEFA compared to Jet A1 experiments.

Figure 16 shows the change of Sauter Mean Diameter with distance from the injector exit. In the figure, calculated value using an empirical equation proposed by El-Shanawany and Lefebvre [15] for the two fuels are plotted. The equation is expressed as follows:

$$\frac{SMD}{D_h} = \left(1 + \frac{1}{AFR}\right) \left[0.33 \left(\frac{\sigma_L}{\rho_A U_A^2 D_p} \right)^{0.6} \left(\frac{\rho_L}{\rho_A} \right)^{0.1} + 0.068 \left(\frac{\mu_L^2}{\sigma_L \rho_L D_p} \right)^{0.5} \right]$$

where SMD is the Sauter Mean Diameter, D_h is the hydraulic diameter of injector exit, D_p is liquid film diameter, U_A is airflow velocity, ρ_L is liquid density, ρ_A is gas density, σ_L is surface tension of liquid, μ_L is viscosity coefficient of liquid, and AFR is mass air fuel ratio.

Figure 17 shows the change of estimated axial velocity with distance from injector exit. This estimation was made using the moving speed of drops in the measurement location.

From Figs. 16 and 17 it can be deduced that measured and estimated Sauter Mean Diameter immediately after the injection was slightly larger for HEFA compared to the case of Jet A1. This indicates that atomization characteristics are better for Jet A1

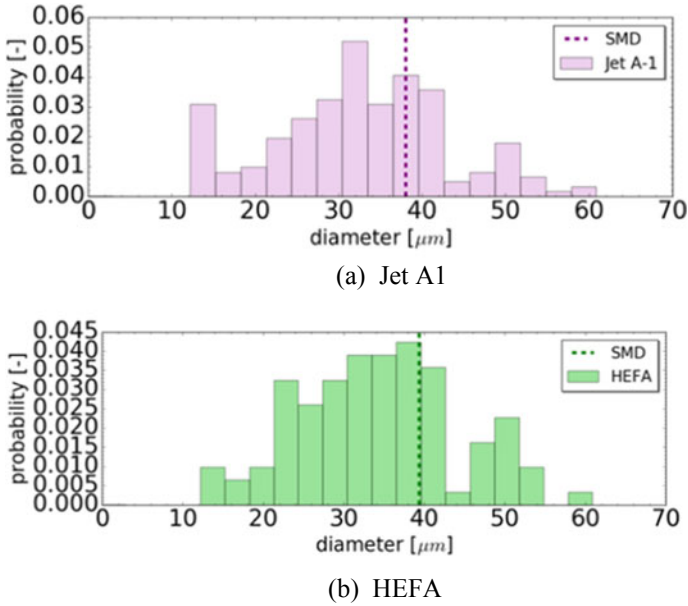


Fig. 15 Droplet diameter distribution at 30 mm downstream from injector exit. **a** Jet A-1, **b** HEFA

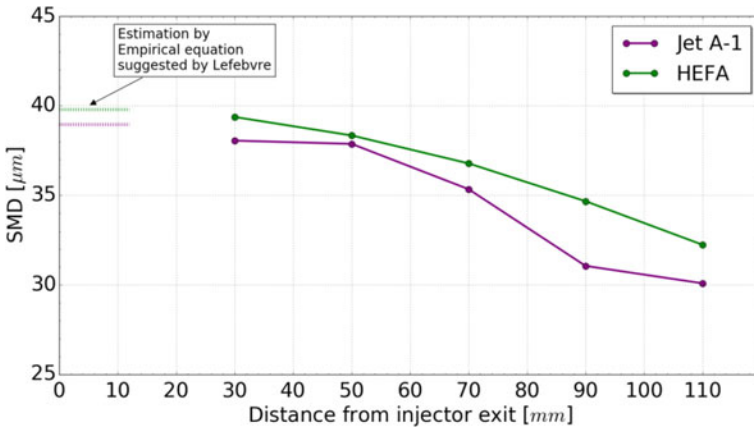


Fig. 16 Change of Sauter Mean Diameter with distance from injector exit

than HEFA. Table 6 shows a summary of the related properties used in the equation for SMD calculation. The slight difference in atomization characteristics comes from the difference of related properties used in the equation.

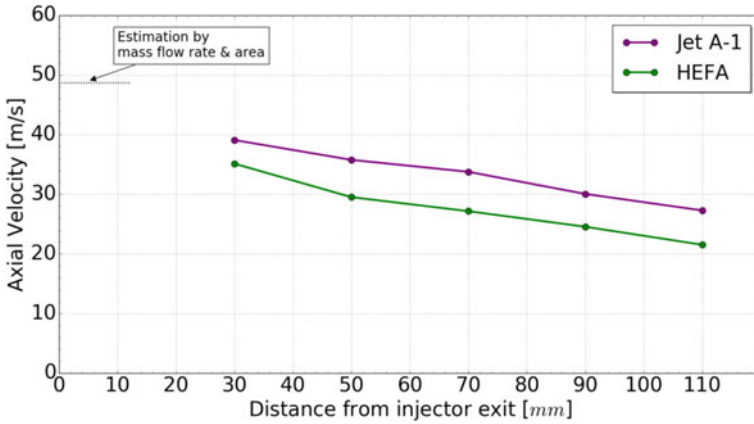


Fig. 17 Change of axial velocity with distance from injector exit

Table 6 Comparison of properties related to the equation by El-Shanawany and Lefebvre (taken from Table 1)

Properties	HEFA	Jet A1
Dynamic viscosity (mm ² /s) @ 15 °C	1.963	1.655
Surface tension (mN/m)	22.5	23.6
Density (g/cm ³) @ 15 °C	0.7554	0.7886

Atomization characteristics are an important factor in determining the combustion stability. Evaporation rate was measured from single droplet evaporation tests in high-temperature vessels. Figure 18 shows an example of back-lit image of an evaporating droplet. This single droplet evaporation test relies on the diameter (d) squared (d^2) law [16]. For the evaporation and combustion of single droplets, the square of the

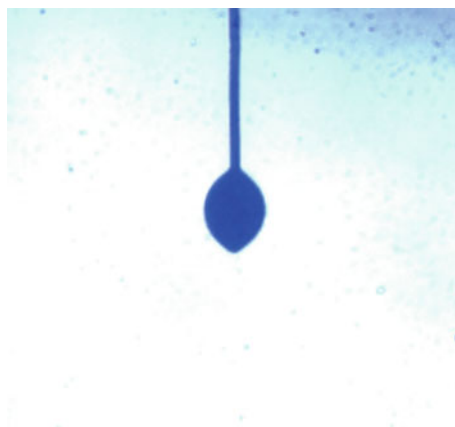


Fig. 18 Appearance of droplet during evaporation testing

droplet diameter changes linearly with time. This constant of proportionality for the evaporation case is called the evaporation rate constant, K_v . This constant, after a short period of initial heat-up period, takes almost no change in value.

Figures 19 and 20 compare the time history of droplet diameter squared and instantaneous evaporation rate constant for Jet A1 and HEFA, respectively. For both fuels, the evaporation rate constant for most of the time takes nearly constant value except the initial and terminating periods. Average values from 40 to 80% of the time progressed were compared and Figs. 19 and 20 show a higher evaporation rate constant for HEFA than for Jet A1. This indicates that evaporation characteristics are better for HEFA than Jet A1 and HEFA is advantageous than Jet A1 in combustion stability point of view. This contrast might come from the difference in the fuel composition and further investigation may be necessary to understand the in-detail mechanism.

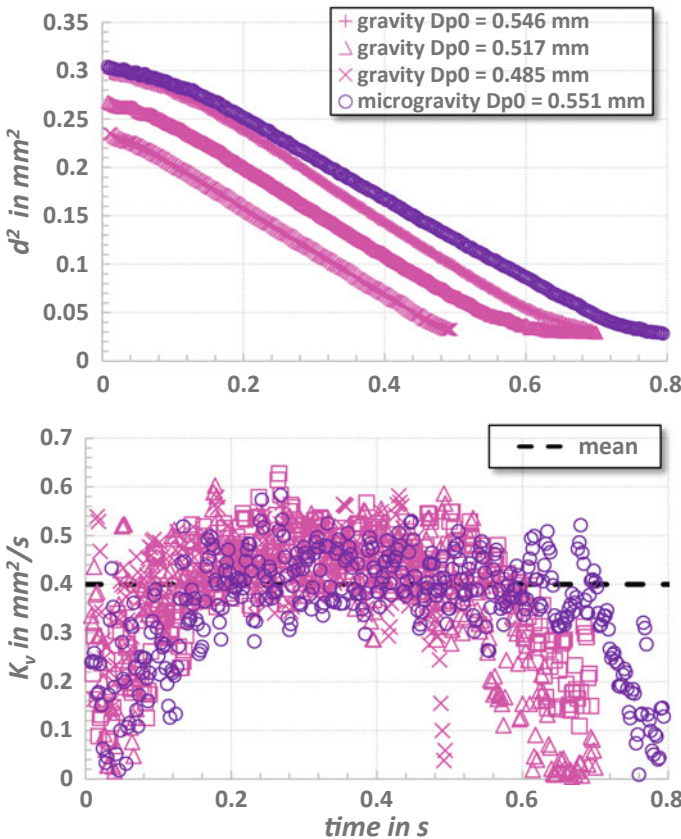


Fig. 19 Time history of droplet diameter squared and instantaneous evaporation rate constant (Jet A1)

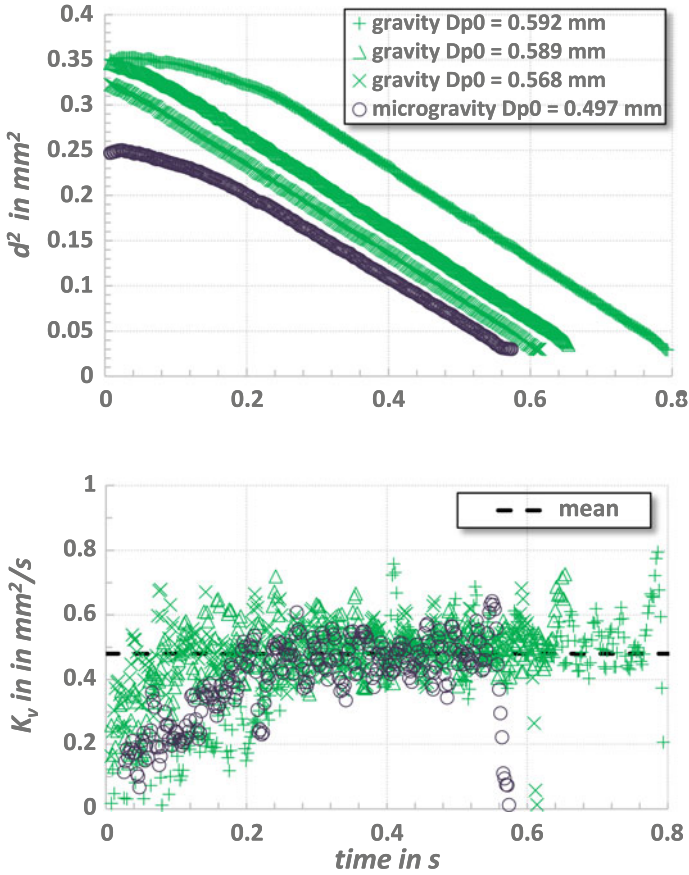


Fig. 20 Time history of droplet diameter squared and instantaneous evaporation rate constant (HEFA)

In addition, Figs. 19 and 20 show the evaporation of a HEFA and Jet A1 droplet at microgravity, respectively. Microgravity experiments are conducted by using the apparatus displayed in Fig. 3 under free-fall conditions. The dropping package can fall for 1.4 s in the 10 m high drop tower of the University of Tokyo (for more information, the authors refer to [17]). Microgravity experiments allow combustion and evaporation without the influence of, e.g., buoyancy effects. The influence of those effects increases with initial droplet size. Although the droplets used for the evaporation experiments are bigger than 0.5 mm in diameter, the gravity and microgravity data match and prove that evaporation data under normal gravity are reliable for the presented conditions.

High-temperature and high-pressure combustion testing at low equivalence ratio conditions was conducted to investigate the flame stability at those conditions. The experiments indicate, that the pressure fluctuation characteristics are clearly different

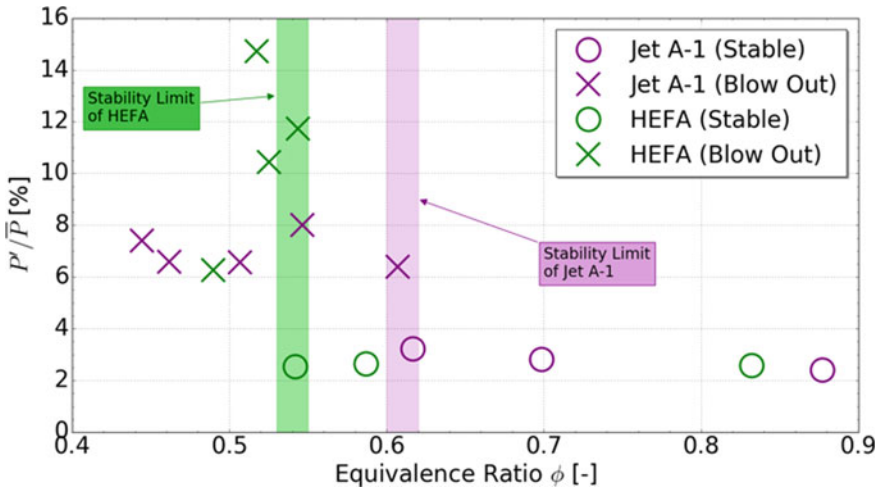


Fig. 21 Combustion stability in the case of high-temperature and high-pressure testing

between the stable combustion and blowout conditions. To compare the pressure fluctuation characteristics, a parameter P' showing the degree of pressure variation is defined as follows:

$$P' = 2|\overline{P_C} - \bar{P}_C|$$

Figure 21 shows the change of the parameter with equivalence ratio for the two fuel types. This figure clearly shows that for both fuels there exists a threshold of stability limit. For the blowout conditions, the pressure fluctuation is more intense than stable combustion conditions. Figure 21 shows that the onset of instability for HEFA as the fuel has a lower equivalence ratio than for Jet A1. In this context, the stable combustion region is wider for HEFA than Jet A1.

It was mentioned that blowout condition in lean combustion regime shows large pressure fluctuation with time than stable combustion condition. These pressure fluctuations are compared in the following.

Figures 22 and 23 show pressure oscillation measured (time history and frequency analysis) at a stable condition ($\phi = 0.87$) for Jet A1 and HEFA, respectively.

Figures 24 and 25 show pressure oscillation measured (time history and frequency analysis) at a blowout condition ($\phi = 0.52$) for Jet A1 and HEFA, respectively.

For the frequency analysis, Power Spectrum Density (PSD) applying Fast Fourier Transform (FFT) was plotted. For the stable combustion case, Figs. 22 and 23 show similar tendencies. Frequency analysis shows several peaks, which resemble both fuel cases. Helmholtz frequency (120 Hz) and axial-direction natural acoustic frequency (1170 Hz) are both observed in the figures.

For the blowout condition, pressure oscillation history and frequency analysis both shows different tendency comparing the two fuel cases. For Jet A1 shown in

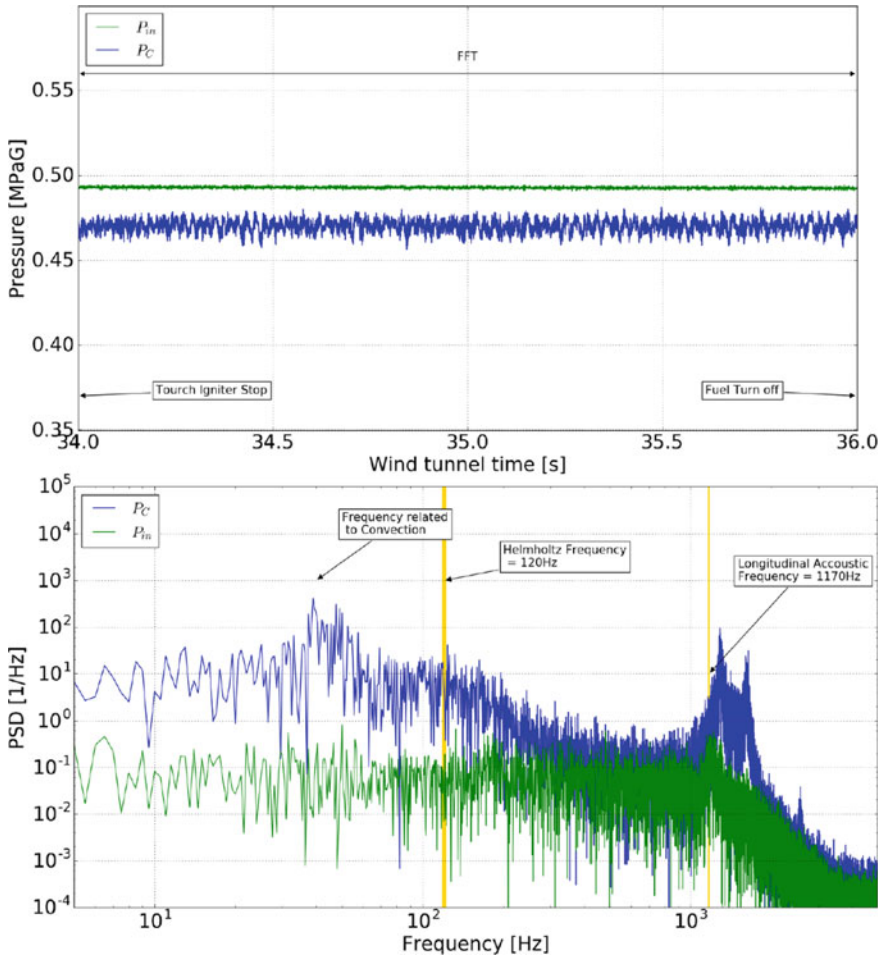


Fig. 22 Pressure oscillation measured (time history and frequency analysis; stable condition ($\phi = 0.87$) and Jet A1 case)

Fig. 24, periodic vibration was observed before onset of blowout. This suggests that the combustion oscillation occurred was related to Helmholtz-type combustion oscillation. On the other hand, pressure history for HEFA fuel case did not show periodic vibration and was almost irregular with time as seen in Fig. 25. Frequency analysis also shows nearly no clear peak, especially in the low-frequency area. To further investigate this irregular flame oscillation, flame behavior is next compared to the two fuel cases.

Figures 26 and 27 show appearances of spray (Mie scattered image) and flame (CH^* chemiluminescence) at unstable combustion conditions ($\phi = 0.52$) for Jet A1 and HEFA, respectively.

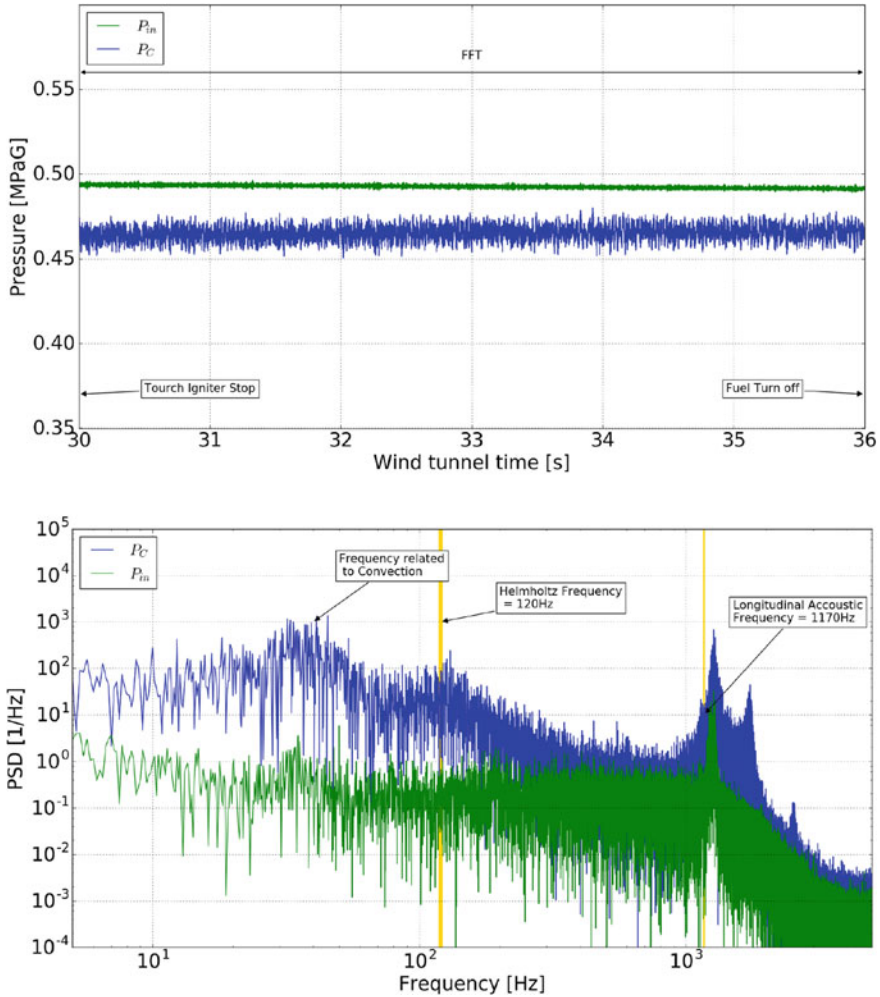


Fig. 23 Pressure oscillation measured (time history and frequency analysis; Stable condition ($\varphi = 0.87$) and HEFA case)

At first, flame appearance shown in Fig. 26 is investigated. Number 1 through 8 shows a flame image for almost 1 period of the periodic oscillation. During the (1) and (2) time period, as the combustion chamber pressure P_C decreases the pressure difference between P_C and incoming air pressure P_{in} increases, and the large pressure difference enhances air entrainment and incoming velocity. This suggests that large amount of fuel spray is introduced due to the large pressure difference. This is in accordance with the following images from (2) to (5) Mie scattered images. Furthermore, an increase in air velocity related to the atomization process might enhance the atomization characteristics. The change of the pressure difference and

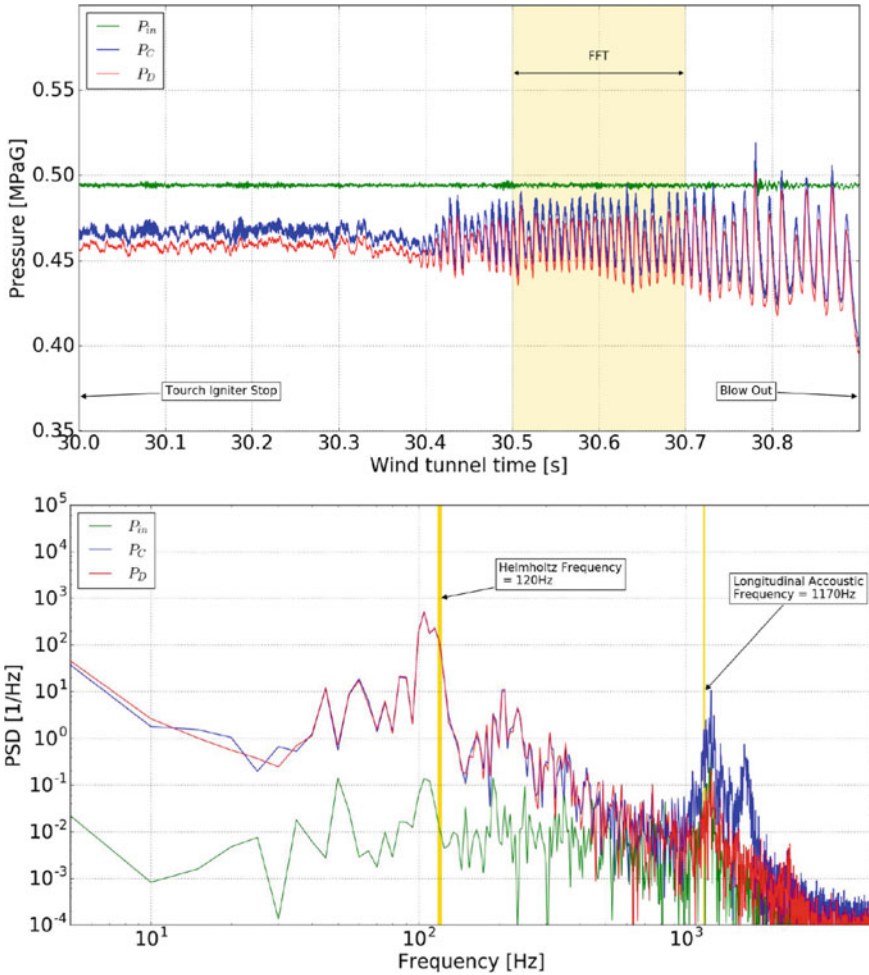


Fig. 24 Pressure oscillation measured (time history and frequency analysis; blow out condition ($\varphi = 0.52$) and Jet A1 case)

the change of the sprays in time has a time delay, and the delay suggests characteristic times for atomization and convection are apparent. CH^* chemiluminescence image from (2) to (7) shows combustion and heat release, thereby time variation of spray and of chemiluminescence also have a time delay. This delay would be related to the time delay due to spray evaporation and chemical reactions. CH^* chemiluminescence images of (5) and (6) are most prominent among the eight images, suggesting that heat release is most intense. In these time period, chamber pressure P_C takes highest value. Phases in variation of heat release and pressure are likely to close each other. Therefore, the oscillation seen in Fig. 24 might be related to the Rayleigh relationship. From these observations, in the case of Jet A1 fuel, the reason for the oscillation

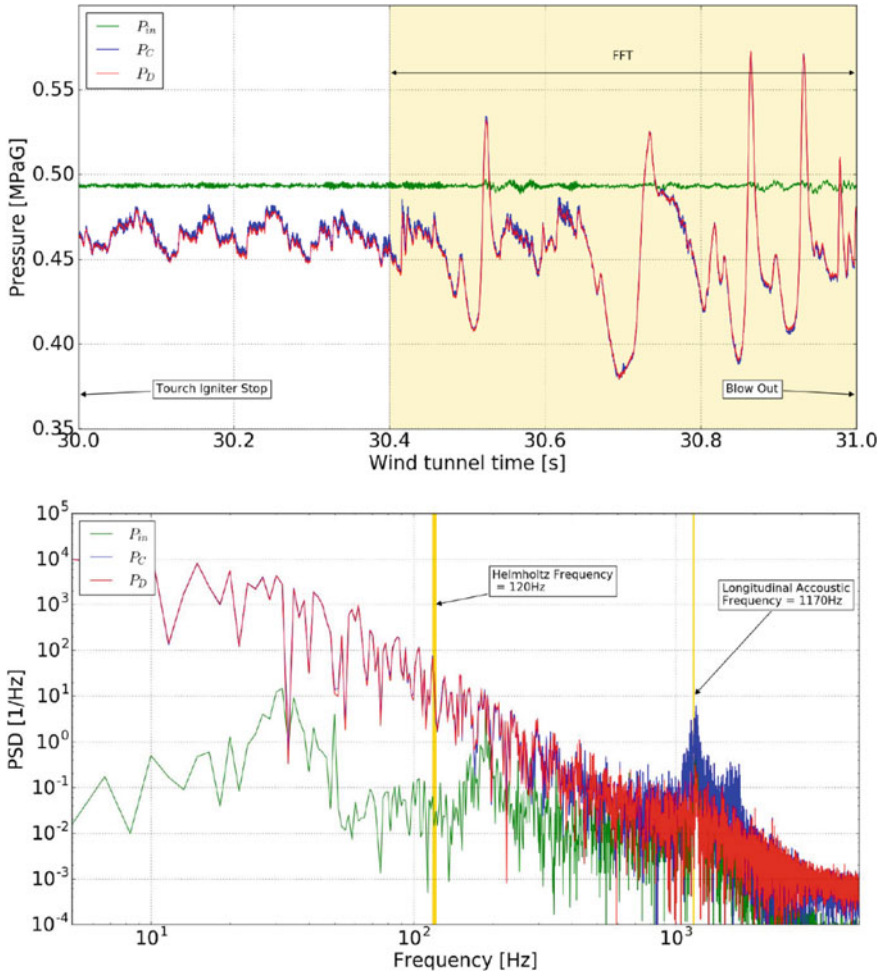


Fig. 25 Pressure oscillation measured (time history and frequency analysis; blow out condition ($\varphi = 0.52$) and HEFA case)

occurrence was the time delay between the pressure and heat release fluctuations was adequate for the excitation of the Helmholtz-type combustion oscillation.

Appearances of spray (Mie scattered image) and flame (CH^* chemiluminescence) at unstable combustion condition ($\varphi = 0.52$) for HEFA seen in Fig. 27 does not show similar causal relationships between spray and chemiluminescence as Jet A1 case seen in Fig. 26.

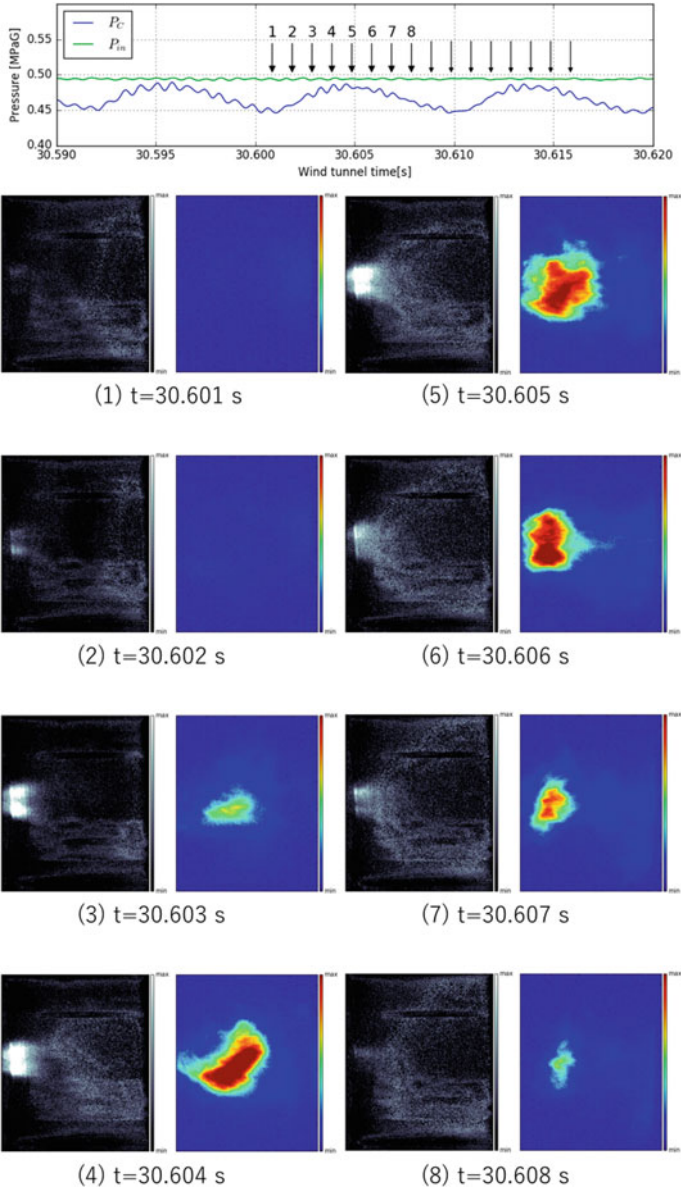


Fig. 26 Appearance of unstable combustion (blow out condition ($\varphi = 0.52$) and Jet A1 case)

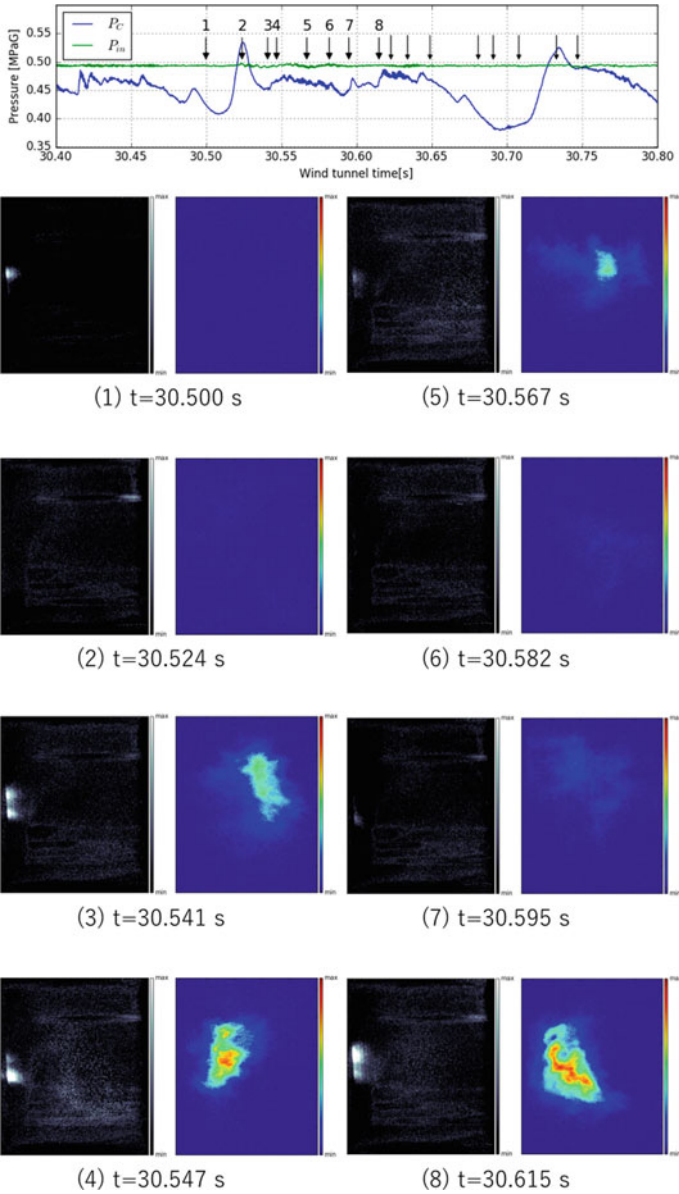


Fig. 27 Appearance of unstable combustion (blow out condition ($\varphi = 0.52$) and HEFA case)

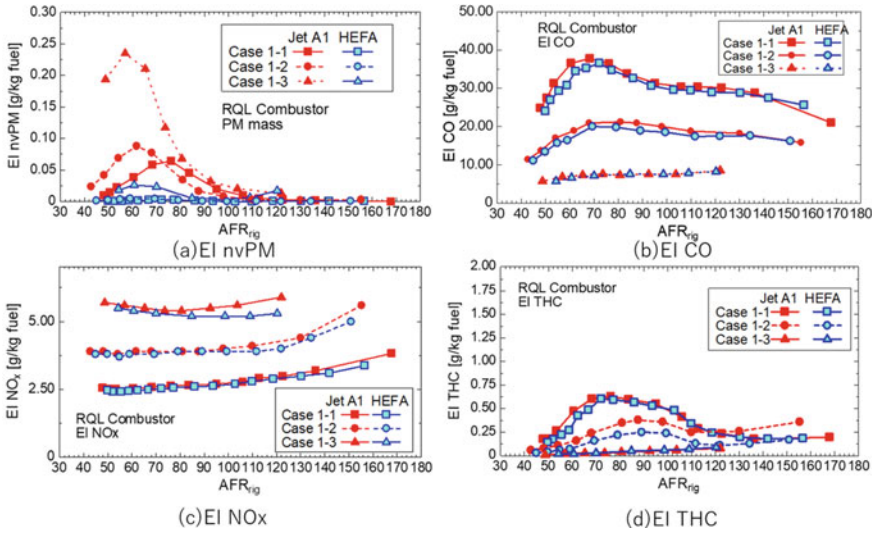


Fig. 28 Emission characteristics for RQL combustor testing (case 1)

3.2 Combustion Testing with RQL Combustor¹

Combustion rig tests were conducted using two different combustors (case 1: rich burn quick quench lean burn, RQL, Combustor, and case 2: Concentric Lean Burn Combustor). The results obtained from RQL combustor are presented at first in this subsection.

Three inlet air conditions (cases 1-1, 1-2, and 1-3) shown in Table 5 were tested with total air/fuel ratios ranged from about 50 to 150. Jet A1 and HEFA were blended before supplying to the fuel nozzle through a T-junction when a mixture of the two fuel was tested.

Combustion tests with each having 100% HEFA and 100% Jet A1 supplied separately were conducted to investigate the effect of the fuel on the combustion behavior. Figure 28 shows the non-volatile PM (nvPM), NO_x, CO, and THC emission index (in g/kg fuel) as a function of the air/fuel ratio.

The result indicates that the nvPM emission index was greatly reduced with HEFA while other exhaust gas components were like each other.

NvPM emission for each fuel increases with the increase of load (pressure and temperature) intensity. EI CO decreases with the increase of load intensity for both fuels, approaching perfect combustion. EI NO_x increases with the increase of pressure and temperature for both fuels. EI THC decreases with the increase of load intensity for both fuels like EI CO, approaching perfect combustion.

¹AIAA 2016-4953 [18] and AIAA2019-1772 [19]: reprinted with permission of American Institute of Aeronautics and Astronautics, Inc.

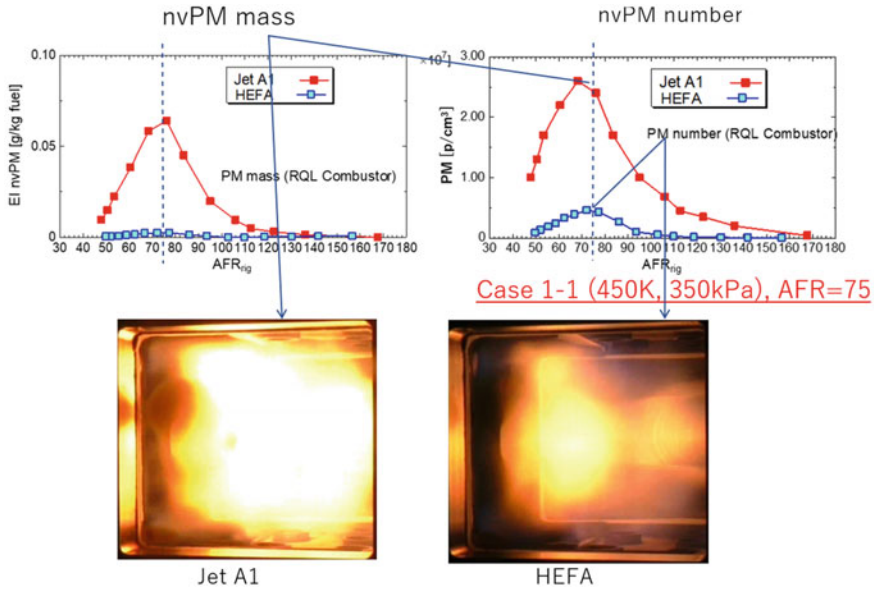


Fig. 29 Comparison of nvPM mass and number (case 1-1; RQL combustor)

Figure 29 shows mass and number of nvPM emission for case 1-1. It also shows that the maximum value of nvPM emission index appeared at the condition of air fuel ratio of approximately 75, wherein 96% reduction of nvPM mass emission index was observed when using HEFA instead of Jet A1, while the peak value of nvPM number with HEFA is about 18% of that with Jet A1. The reduction of nvPM mass with HEFA was more critical than the number of nvPM, indicating that large size nvPMs are decreased with HEFA than Jet A1 and the average size of nvPM with HEFA is smaller than that with Jet A1.

Figure 29 also compares the direct flame images at air fuel ratio of 75 with HEFA and Jet A1 images captured from outside of the pressure chamber by a usual digital camera without changing any conditions of the camera including the aperture. The images show that HEFA had less flame brightness than that from Jet A1 combustion; this is consistent with the above results of the reduced nvPM emission (both on mass and number) when using HEFA. Figure 30 shows spatial distribution of soot showing the KL factor determined using Hottel and Broughton two-color radiometry. KL factor in Jet A1 flame shows a region having large value of KL factor around luminous flame and on the other hand, KL factor in HEFA flame shows smaller value than Jet A1 case. Change of KL factor with the increase of AFR shows a similar tendency with nvPM mass and number.

In order to further examine the effect of the blending ratio of the two fuels to the exhaust gas emission index, the blending ratio of HEFA were changed in increments of 10%, keeping the air fuel ratio at 75. The result is shown in Fig. 31. The results show that both nvPM mass emission index and number density were reduced with

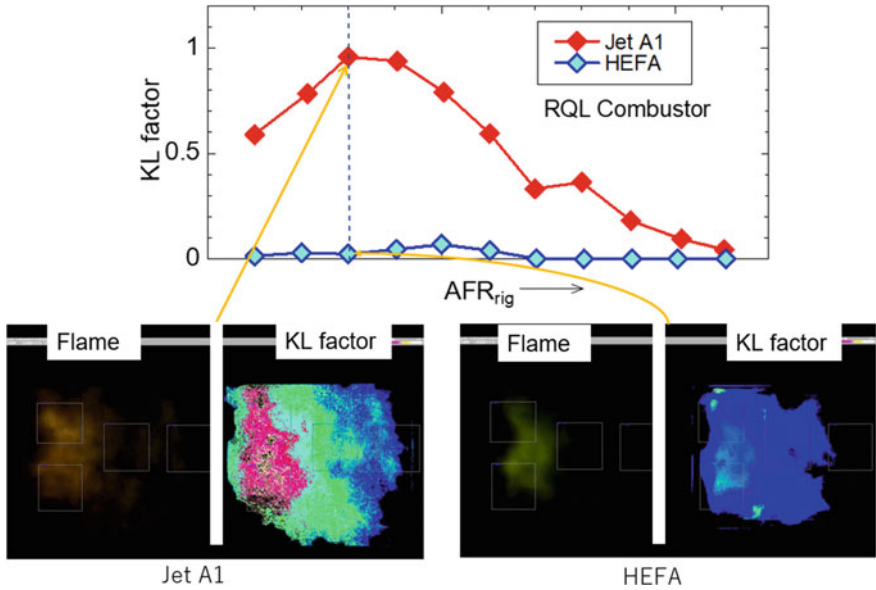


Fig. 30 KL factor taken from Hottel and Broughton two-color radiometry (RQL combustor)

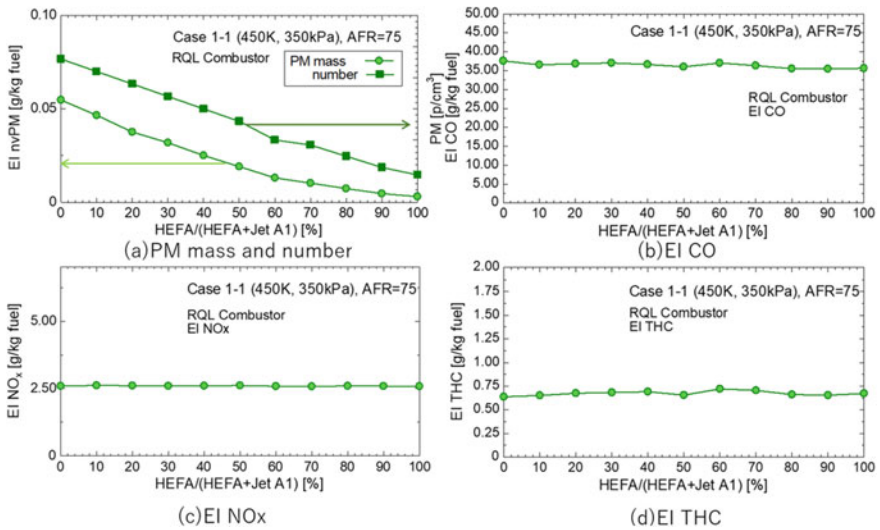


Fig. 31 Effect of fuel composition on emission characteristics (case 1-1; RQL combustor)

an increase in HEFA blend ratio while NO_x , CO and THC remained constant. The decrease rate of nvPM mass and number with an increase of HEFA content in mixture fuel look slightly different by each other. This difference in emission indices and soot distribution would be important for the different mechanisms of agglomeration and perhaps different impacts on environment (through cirrus formation), which requires further investigation.

3.3 *Combustion Testing with Concentric Lean Burn Combustor*²

The results obtained from concentric lean burn combustor are presented in this subsection.

Case 2-1 and cases 2-2 and 2-3 were different in fuel injection schedule. In case 2-1 only pilot fuel was injected, which represents a low load condition. Cases 2-2 and 2-3 had both pilot and main fuel injected and represents a high load condition.

Figure 32 compares the two different fuel injection schedules.

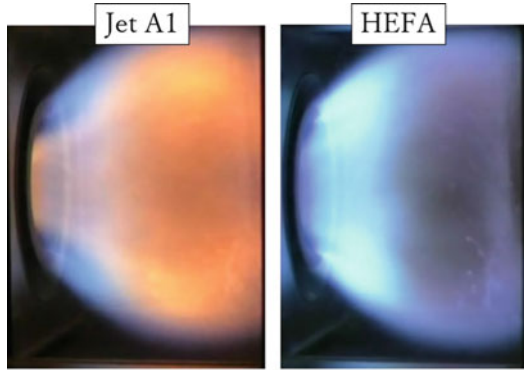
In the results of case 2-1 (pilot only), air fuel ratio was 100 and direct flame images of the condition with pure fuel (both Jet A1 and HEFA) were compared as shown in Fig. 32 (upper side). A blue flame was dominant with HEFA, while a yellow flame was dominant with Jet A1. In case 2-2, both pilot and main burner were fueled. In a previous study, a combustion instability was observed, and its phenomena were reported, when the same combustor and injector configuration were used [21]. As expected, in the present study with Jet A1 as fuel, combustion instability was observed at a pilot fuel ratio of up to 15% (case 2-3). Initially, the fuel injection condition without inducing instability was examined. No combustion instability was observed when the pilot fuel ratio was at 20% for both pure fuel cases (Jet A1 and HEFA). The bottom side of Fig. 32 shows a comparison of the direct flame images when the pilot fuel ratio was 20% and air fuel ratio was 35 (stable combustion condition). The results showed that both main and pilot flames are blue when HEFA was used, while the main flame was blue, and the pilot flame was yellow when Jet A1 was used as fuel.

In the case of no instability cases [Case 2-1 (pilot only) and 2-3 (pilot fuel ratio was 20%)], the emission indices were compared in Fig. 33, indicating that NO_x , THC, and CO emission were like each other. Non-volatile PM was much smaller than in case 2-1, with only the pilot burner operational. A similar tendency was also observed for the cases 1-1 through 1-3 with RQL combustor given earlier in this chapter.

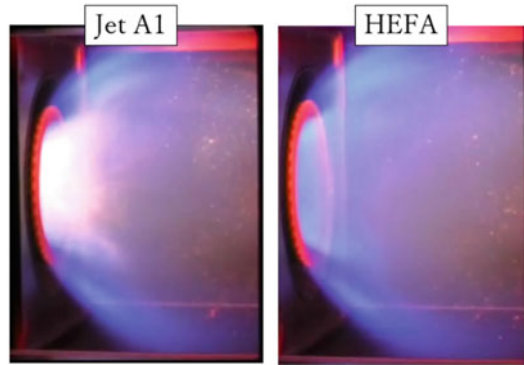
Figure 34 shows a comparison of NO_x emission between the two fuels under the condition of both stable and instable combustion observed in the Jet A1 case (only pilot fuel ratio is different). Figure 34 also shows the stated pressure oscillation,

²AIAA 2018-1474 [20]: reprinted with permission of American Institute of Aeronautics and Astronautics, Inc.

Fig. 32 Comparison of the direct flame images (lean burn combustor cases 2-1 and 2-2)



Case 2-1 Pilot only case (pilot burner only, AFR = 100)



Case 2-2 Pilot and main burner case (AFR ~ 35)

as measured using a pressure transducer located on the liner wall at the condition where air fuel ratio was 40.7, pilot fuel ratio was 15% and Jet A1 was used as the fuel (top left side of the figure on the bottom). The upper figures on the bottom show time-dependent pressure oscillation while the lower show spectrum of oscillation. The figure shows a pressure oscillation of around 550 Hz using Jet A1 fuel. Right side at the bottom of Fig. 34 shows the same pressure oscillation as mentioned above (with Jet A1) at the condition when air fuel ratio was 38.5, pilot fuel ratio was 15% using HEFA as the fuel. In the HEFA test, no oscillation was observed under any condition as seen from the figure.

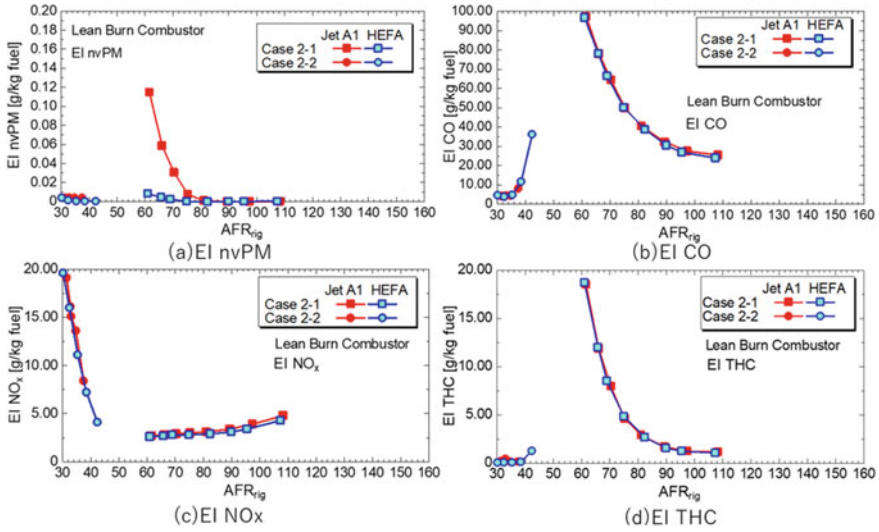


Fig. 33 Emission characteristics for lean burn combustor testing (cases 2-1 and 2-2)

3.4 Discussions

Combustion test cases in which spray and diffusion flame region are dominant, the effect of fuel change from Jet A1 to HEFA is remarkable especially in soot-formation phenomena. The results showed clear reduction of Emission Index (EI) nvPM and number density nvPM for HEFA and mixture fuels compared to pure Jet A1 and this is attributed largely to the reduced aromatic concentration [5]. This tendency was also verified through KL factor distribution taken from Hottel and Broughton two-color radiometry, which is related to soot concentration spatial distribution. Comparison between nvPM mass and number indices, it was suggested that HEFA fuel reduces PM mass but the rate of decrease in number nvPM was less than that in mass, indicating a large number of smaller particles formed. These might affect the ability to form early stage of cirrus cloud. Further, in-detail investigation is necessary.

The other combustion properties, EI of CO, NO_x and THC were almost unaffected by the fuel change. In case 2-3, an unstable condition exhibited when using Jet A1, but no visible instability occurred when using HEFA in the same condition. This might be from the slight differences in atomization behavior due to different properties, such as density and surface tension.

In the present combustor rig test, the fuel composition was well within the stable combustion regime with respect to the lean blowout. Fuel injector testing investigated those lean blowout conditions. The test results showed a slight wider stability regime obtained for HEFA than for Jet A1. This result is in accordance with the consideration given by Corporan and co-workers [22]. Edwards and co-workers [23] evaluated the effect of fuel properties on LBO in the same combustor and the same environment

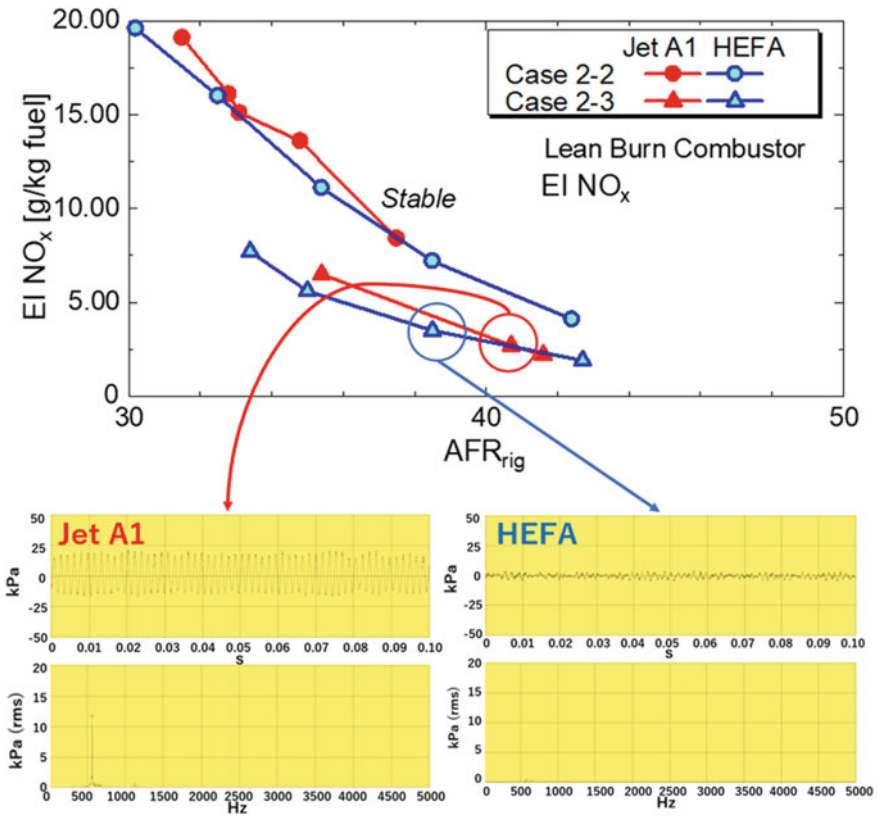


Fig. 34 Stable and unstable combustion in lean burn combustor (cases 2-2 and 2-3)

referencing a phenomenological model developed by Lefebvre [24] as follows:

$$\varphi_{LBO} = \left[\frac{f_{pz}}{V_{pz}} \right] \left[\frac{\dot{m}_A}{P_3^{1.3} \exp(T_3/300)} \right] \left[\frac{D_0^2}{\lambda_{eff} LCV} \right]$$

The first term of the right side of the equation is a function of combustor design. The second term represents the operating conditions. The last term embodies the relevant fuel properties, D_0 , λ , and LCV, the diameter of the fuel spray, the evaporation constant, and lower heating value for the fuel, respectively. If the experiments only changed fuels, the ratio φ_{LBO} becomes a ratio of the fuel properties. Ratio of properties utilizing the present results are

- $(D_0|_{JetA}/D_0|_{HEFA}) = 0.97$ (From SMD in Figs. 15 and 16)
- $(\lambda_{eff}|_{JetA}/\lambda_{eff}|_{HEFA}) = 0.85$ (From Evaporation constant, in Figs. 19 and 20)
- $(LHV|_{JetA}/LHV|_{HEFA}) = 0.98$ (From Heat of Combustion in Table 1).

From these ratios, the ratio of ϕ_{LBO} from the above equation becomes 1.13. This is in accordance with the present results shown in Fig. 21.

In the previous report using the same combustor [21], a simple acoustic velocity coupling mechanism was proposed as the driving mechanism to generate heat release oscillations which were used to explain the observed oscillation. In the proposed mechanism, there were coupled features inducing the oscillation, including the path of “fuel atomization, evaporation, and mixing.”

As explained by Lefebvre and Ballal [5], “the time between the injection of fuel and the region of maximum heat release represents the characteristic combustion time, which is obtained as the sum of the characteristic times for the fuel evaporation, mixing of fuel vapor with air and combustion products to reach a critical reaction temperature and chemical reaction. The system becomes prone to instabilities when the overall combustion time becomes equal to a characteristic acoustic time of the combustor.”

Additional measurements of Sauter Mean Diameter indicated that atomization characteristics are slightly better for Jet A1 than HEFA. Evaporation characteristics were better for HEFA than Jet A1 and HEFA is advantageous than Jet A1 in combustion stability point of view. The autoignition characteristics of the conventional jet fuel and alternative jet fuel were investigated using a rapid compression machine by Allen and co-workers [25]. The result showed that alternative fuels ignited more readily than conventional fuels for all tested conditions. This suggests that higher chemical reactivity for HEFA than Jet A1. Overall, among the characteristic times, HEFA is advantageous for some aspects and disadvantageous for others than Jet A1. It was suggested that the slightly different physical properties (density and surface tension) might affect the liquid atomization characteristics for the two fuels. Other characteristics are also affected by the slight difference between physical and chemical properties and conditions. In the unstable combustion seen in lean burn combustor case, a slight difference in fuel properties changed the onset condition of instability.

By introducing HEFA and bio-derived fuels to aviation, the results showed carbon emission reduction that shifted towards carbon-neutrality. If the upper limit of alternative fuels in mixtures for aviation propulsion is increased, the contribution to reduce carbon emission would be enhanced. From these investigations, major issues associated with increasing the ratio of, e.g., HEFA in the fuel mixture above 50% would be the cause in swelling of O-rings, a different energy content due to different density, etc. These drawbacks seem technically solvable in the medium-term perspective. Other than lean blowout conditions, cold start and altitude ignition [26] might be important for the confirmation of wider use of these alternative fuels for aviation.

4 Conclusion

In this chapter, several important aspects of original aviation fuel (Jet A1) and an alternative aviation fuel (HEFA) were compared and investigated.

Chemical and physical property analysis and combustion rig test with two different combustor types were performed and investigated using both fuels and their blends.

The exhaust gas measurement data showed that the non-volatile PM mass reduced when using HEFA and its blends with Jet A1, which was also supported by the flame visualization studies.

Non-volatile particulate matter (nvPM) mass was reduced with HEFA only at pilot mode for the concentric lean burn burner, while NO_x , THC, and CO emissions were similar between the two fuels.

Combustion instabilities were observed with Jet A1 under certain conditions of pilot and main fuel injection mode for the concentric lean burn burner, while those were not observed with HEFA at any conditions within the present test conditions examined. Fuel changes may affect combustion instability characteristics.

Acknowledgements This work was in part supported by JSPS KAKENHI Grant Number 16H04586.

The authors thank Professor Ashwani K. Gupta of the University of Maryland for his comments and revisions.

References

1. National Academies of Sciences, Engineering, and Medicine (2016) Commercial aircraft propulsion and energy systems research: reducing global carbon emissions. The National Academies Press, Washington, DC. <https://doi.org/10.17226/23490>
2. ASTM D7566-18 (2018) Standard specification for aviation turbine fuels containing synthesized hydrocarbons. ASTM International, West Conshohocken, PA
3. Fukuyama Y, Fujiwara H, Okai K (2009) Alternative fuels and their impact on the turbofan engine design and performance under the realistic flight conditions. In: ACGT paper no. 51, Asian joint congress on gas turbines 2009 (ACGT 2009), Tokyo, Japan 2009 (ACGT2009-051)
4. Okai K, Fujiwara H, Hongoh M, Shimodaira K (2012) Application of a bio-fuel to a single sector combustor for an experimental small aero-engine. In: Asian joint congress on gas turbines 2012 (ACGT 2012), Shanghai, China, 2012 (ACGT 2012-2121)
5. Lefebvre AH, Ballal DR (2010) Gas turbine combustion: alternative fuels and emissions, 3rd edn. CRC Press, Taylor & Francis, New York
6. Mitsubishi-Hitachi Power Systems (2017) An activity of R&D and verification of bio fuel production—a pilot-scaled testing of throughflow production process (in Japanese). <http://www.nedo.go.jp/content/100870869.pdf>. Accessed 03 Sept 2018
7. Abe Y, Toba M, Mochizuki T, Yoshimura Y (2009) Oxidative degradation behaviour of fatty acid methyl ester in fish oil biodiesel and improvement of oxidation stability by partial hydrogenation. *J Jpn Pet Inst* 52(6):307–315 (in Japanese)
8. Glover AR, Skippon SM, Boyle RD (1995) Interferometric laser imaging for droplet sizing: a method for droplet-size measurement in sparse spray systems. *Appl Opt* 34(36):8409
9. Shigeta Y, Hayashi K, Ichiyana M, Hishida K (2012) Measurement of droplet size, velocity and spatial distribution of mass flux in spray by combining focus and defocus imaging technique. *Trans Jpn Soc Mech Eng Ser B* 78(788):867–880
10. Maeda M, Kawaguchi T, Hishida K (2000) Novel interferometric measurement of size and velocity distributions of spherical particles in fluid flows. *Meas Sci Technol* 11:L13–L18

11. Nakaya S, Fujishima K, Tsue M, Kono M, Segewa D (2013) Effects of drop-let diameter on instantaneous burning rate of isolated fuel droplets in argon-rich or carbon dioxide-rich ambiances under microgravity. *Proc Combust Inst* 34(1):1601–1608
12. Hottel HC, Broughton FP (1932) *Ind Eng Chem* 4(2):166–174
13. Makida M, Yamada H, Shimodaira K (2014) Detailed research on rich-lean type single sector and full annular combustor for small aircraft engine. In: 29th congress of the international council of the aeronautical sciences (ICAS 2014), St. Petersburg, Russia (ICAS2014-0628)
14. Yamamoto T, Shimodaira K, Yoshida S, Kurosawa Y (2013) *J Eng Gas Turb Power* 135:031502
15. El-Shanawany MS, Lefebvre AH (1980) Airblast atomization: effect of linear scale on mean drop size. *J Energy* 4(4):184–189
16. Spalding DB (1953) The combustion of liquid fuels. *Symp Combust* 4(1):847–864
17. Ando S, Wu Y, Nakaya S, Tsue M (2020) Droplet combustion behavior of oxidatively degraded methyl laurate and methyl oleate microgravity. *Combust Flame* (in press)
18. Okai K, Fujiwara H, Makida M, Shimodaira K, Yamada H, Namakura M (2016) The effect of the fuel change from petroleum kerosene to HEFA alternative jet fuel on the emission of an RQL type gas turbine combustor. In: 14th international energy conversion engineering conference, AIAA propulsion and energy forum (AIAA 2016-4953)
19. Okai K, Fujiwara H, Makida M, Shimodaira K (2019) The effect of the fuel change from petroleum kerosene to HEFA alternative jet fuel on the number of nvPM emission of an RQL gas turbine combustor. In: AIAA aerospace science meeting, AIAA SciTech Forum (AIAA 2019-1772)
20. Okai K, Fujiwara H, Yoshida S, Yamamoto T, Shimodaira K (2018) The effect of the fuel change from petroleum kerosene to HEFA alternative jet fuel on the emission of a concentric lean-burn burner for gas turbine. In: AIAA aerospace science meeting, AIAA SciTech Forum (AIAA 2018-1474)
21. Tachibana A, Saito K, Yamamoto T, Makida M, Kitano T, Kurose R (2015) Experimental and numerical investigation of thermo-acoustic instability in a liquid-fuel aero-engine combustor at elevated pressure: validity of large-eddy simulation of spray combustion. *Combust Flame* 162:2621–2637
22. Corporan E, Edwards T, Stouffer S, Hendershott T, DeWitt M, Klingshirn C, West Z, Bruening C, Striebich R (2017) Impacts of fuel properties on combustor performance, operability, and emissions characteristics, 55th AIAA aerospace science meeting, Grapevine, Texas (AIAA 2017-0380)
23. Edwards T, Moses C, Dryer F, Evaluation of combustion performance of alternative aviation fuels. In: 46th AIAA/ASME/SAE/ASEE joint propulsion conference & exhibit, Nashville, Tennessee (AIAA 2010-7155)
24. Lefebvre AH (1985) Fuel effects on gas turbine combustion—ignition, stability and combustion efficiency. *J Eng Gas Turbines Power* 107:24–37
25. Allen C, Toulson E, Edwards T, Lee T (2013) Ignition behaviour and surrogate modelling of JP-8 and of camelina and tallow hydrotreated renewable jet fuel at low temperatures. *Combust Flame* 160(2):232–239
26. Heyne JS, Colket M, Gupta M, Jardines A, Moder J, Edwards JT, Roquemore WM, Li C, Rumizen M, Year 2 of the national jet fuels combustion program: moving towards a streamlined alternative jet fuels qualification and certification process. In: 55th AIAA aerospace science meeting, Grapevine, Texas (AIAA 2017-0145)